Chapter 11
Modeling Regular Aggregate Interference by Symmetric Structures

Markus Rupp, Stefan Schwarz and Martin Taranetz

In this chapter, downlink co-channel interference statistics in wireless cellular networks with hexagonal grid layout are investigated. The main target is to facilitate the analysis at user locations outside the center of the cell of interest.

The proposal of a cellular structure for mobile networks dates back to 1947. Two Bell Labs engineers, Douglas H. Ring and W. Rae Young were the first to mention the idea in an internal memorandum [1]. Almost two decades later, in 1966, Richard H. Frenkiel and Philip T. Porter, shaped a *hexagonal cellular array of areas* to propose the first mobile phone system. Although never proposed as innovative research solution, the hexagon model gained high popularity within the research community and is still extensively utilized nowadays [2–7]. It serves either as the system model itself, or as a reference system for more involved simulation scenarios. On the other hand, its geometric structure renders closed-form analysis of *aggregate interference statistics* difficult [8]. Hence, simulation results often lack a mathematical back up.

Recently, closed-form results have been reported with system models based on stochastic geometry [9–11]. The stochastic approach is based on an ensemble of network realizations and is therefore not applicable when a fixed structure of the network is given. Since the *well-planned* deployment of macro-sites is not expected to vanish in the medium term, it is thus considered imperative to make interference analysis in the hexagonal grid model more convenient.

Current work on regular grid models has mainly focused on link-distance statistics [12, 13]. The authors also account for fading and provide closed-form approximations for the co-channel interference of a *single link*. However, convenient expressions

M. Rupp (✉) · S. Schwarz · M. Taranetz
Institute of Telecommunications, TU Wien, Vienna, Austria
e-mail: mrupp@nt.tuwien.ac.at

S. Schwarz
e-mail: sschwarz@nt.tuwien.ac.at

M. Taranetz
e-mail: martin.taranetz@tuwien.ac.at

for the moments and the distribution of *aggregate co-channel interference* are not available yet.

Based on the work in [14, 15], the contributions of this chapter are:

- A *circular interference model* to facilitate interference analysis in cellular networks with regular grid layout is introduced. Particular focus is placed on the hexagonal grid due to its ubiquity in wireless communication engineering [2–7]. The key idea is to consider the power of the interfering BSs as being uniformly spread along the perimeter of the hexagon.
- It is proposed to model interference statistics in a hexagonal scenario by a single Gamma Random Variable RV. Its shape- and scale parameters are determined in closed form by employing the *circular model*. The analysis yields key insights on the formative components of the interference distribution. A scenario with regularly arranged macro-sites and randomly distributed small cells demonstrates the model's expedient application in heterogeneous cellular networks.

The chapter forgoes hexagonal grid setups with more than one ring of interferers as well as further performance analysis, which is enabled by the Gamma approximation. Both are considered straightforward and of no particular relevance for this thesis.

The remainder of this chapter is structured as follows: Sect. 11.1 provides preliminaries on the Gamma distribution. Section 11.2 specifies the hexagonal reference-system model. In Sect. 11.3 the circular interference model and its dual pendant are introduced. Section 11.4 investigates Gamma-distributed interference and its parametrization by the proposed circular interference model. In Sect. 11.5, the accuracy of the Gamma approximation is verified. In Sect. 11.6, the circular model is applied for modeling the interference from the macro BSs in a two-tier heterogeneous cellular network. Section 11.7 provides a comparison of the circular model against Long Term Evolution-Advanced LTE-A system level simulations. Section 11.8 concludes the chapter.

11.1 Preliminaries on the Gamma Distribution

In the current- as well as the subsequent chapter, particular focus is placed upon the Gamma distribution due to its wide range of useful properties for wireless communication engineering, some of which are outlined in this section.

The Probability Density Function (PDF) of a Gamma distributed RV X with *shape parameter k* and *scale parameter θ*, i.e., $G \sim \Gamma[k, \theta]$, is defined as

$$f_G(x) = \frac{1}{\theta^k \Gamma(k)} x^{k-1} e^{-x/\theta}. \tag{11.1}$$

Its mean and variance are given by $\mathbb{E}[G] = k\theta$ and $\mathrm{Var}[G] = k\theta^2$.

The Gamma distribution exhibits the *scaling property*, i.e., if $G \sim \Gamma[k, \theta]$, then $aG \sim [k, a\theta]$, $\forall a > 0$, and the *summation property*, i.e., if $G_i \sim \Gamma[k_i, \theta]$ with $i = 1, 2, \ldots, N$, then $\sum_{i=1}^{N} G_i \sim \Gamma[\sum_{i=1}^{N} k_i, \theta]$.

Consider an arbitrary distribution with mean ν and variance σ^2. Then, the distribution $\Gamma[k, \theta]$ with the same first- and second order moments has the parameters

$$k = \frac{\nu^2}{\sigma^2}, \quad \theta = \frac{\sigma^2}{\nu}. \tag{11.2}$$

These simple moment-matching identities can be exploited for accurately approximating fading distributions [16], such as generalized-K [17, 18] and log-normal [16–19], as well as aggregate interference statistics [11, 20, 21].

Additionally, the Gamma distribution covers the power fading distribution of various single- and multi-antenna schemes under the Rayleigh fading assumption. Conventional Single-Input Single-Output (SISO) yields an exponential distribution $\text{Exp}[1/\theta]$, which is equivalent to $\Gamma[1, \theta]$. The power fading of Maximum Ratio Transmission (MRT) with N_{Tx} transmit antennas and one receive antenna can be modeled by $\Gamma[N_{\text{Tx}}, \theta]$, Maximum Ratio Combining (MRC) with one transmit antenna and N_{Rx} receive antennas is characterized by $\Gamma[N_{\text{Rx}}, \theta]$. Furthermore, MRC is often studied in the presence of Nakagami-m fading. Let $Y \sim \text{Nakagami}[m, \Omega]$ and $G = Y^2$. Then, $G \sim \Gamma[m, \Omega/m]$.

According to [22], the quotient $\gamma = S/I$ of two RVs $S \sim \Gamma[k_S, \theta_S]$ and $I \sim \Gamma[k_I, \theta_I]$ is distributed as

$$f_\gamma(x) = \frac{(\theta_I/\theta_S)^{k_S}}{B(k_S, k_I)} \left(1 + \frac{\theta_I}{\theta_S}x\right)^{-k_S-k_I} x^{k_S-1}, \; x > 0 \tag{11.3}$$

with $B(\cdot, \cdot)$ denoting the Beta function. Interpreting γ as a Signal-to-Interference Ratio (SIR) allows to determine the success probability $\mathbb{P}[\gamma > \delta]$ for a given threshold δ as

$$\mathbb{P}[\gamma > \delta] = \frac{\Gamma(k_S + k_I)}{\Gamma(k_S)} \left(\frac{\theta_S}{\delta\,\theta_I}\right)^{k_I} {}_2\bar{F}_1\left(k_I, k_S + k_I, 1 + k_I, -\frac{\theta_S}{\delta\,\theta_I}\right), \tag{11.4}$$

where ${}_2\bar{F}_1(\cdot, \cdot, \cdot, \cdot)$ is a regularized hypergeometric function [11].

These observations motivate the application of the Gamma RV as a sensible compromise between accuracy and tractability. Further properties of Gamma RVs will be discussed as needed.

11.2 Hexagonal Reference Model

The reference hexagonal setup is composed of a central cell and six interfering BSs, as shown in Fig. 11.1. The interferers are equipped with omnidirectional antennas and are located at the edges of a hexagon with radius R (marked as '+' in Fig. 11.1). All BSs are assumed to transmit with the same power. The signal from the ith interfering BS with polar coordinates (R, Ψ_i) to a user with polar coordinates (r, ϕ) experiences macroscopic path loss and fading. It is assumed that $0 < r \leq R/2$, so as to assure

Fig. 11.1 System model.
Center cell with user at
(r, ϕ). Interfering BSs are
located at (R, Ψ_i), where
$\Psi_i = 2\pi i/M$, $i = 1, \ldots, M$
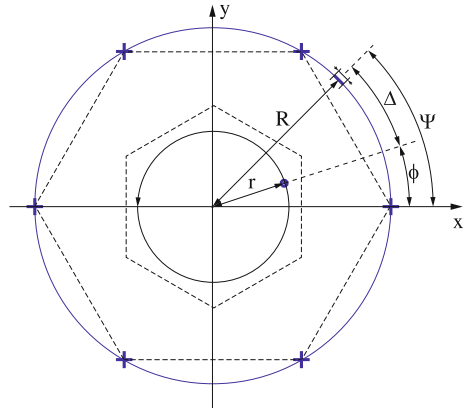
that the user is associated with the central BS. The path loss is modeled by the
exponential law

$$\ell\left(d_{r,\Delta_i}^{(M)}\right) = \min\left(b_\mathrm{P}, \frac{1}{c_\mathrm{P}}\left(d_{r,\Delta_i}^{(M)}\right)^{-\alpha}\right), \tag{11.5}$$

where b_P denotes the intercept, c_P is a constant, α refers to the path loss exponent
and

$$d_{r,\Delta_i}^{(M)} = \sqrt{R^2 + r^2 - 2Rr\cos(\Delta_i)}, \tag{11.6}$$

with $\Delta_i = \phi - \Psi_i$ and $\Psi_i = 2\pi i/M$, $i = 1, \ldots, M$. In the remainder of this chapter,
it is assumed that $d_{r,\Delta_i}^{(M)} > (b_\mathrm{P}c_\mathrm{P})^{-1/\alpha}$. Exemplifying from [23], a minimum coupling
loss of 70 dB and free space propagation at an LTE-A frequency of $f_\mathrm{c} = 2.14$ GHz
yield $b_\mathrm{P} = 10^{-7}$, $c_\mathrm{P} = 8.05 \times 10^{-3}$ and $(b_\mathrm{P}c_\mathrm{P})^{-1/\alpha} = 0.028$ m, hence justifying this
assumption.

In the hexagonal scenario, $M = 6$. The terms r and Δ_i denote the user's distance
to the center and its angle-difference to the ith interfering BS, respectively. Motivated
by Sect. 11.1, fading is modeled by an independent and Identically Distributed (I.I.D.)
Gamma RV $G_i \sim \Gamma[k_0, \theta_0]$, where k_0 and θ_0 refer to shape- and scale parameter,
respectively.

11.3   Circular Interference Model

In a one-tier hexagonal grid scenario, as presented in Sect. 11.2, the experienced
aggregate interference power at position (r, ϕ) can be expressed as

$$I_6(r, \phi) = \sum_{i=1}^{6} P_\mathrm{M}\, G_i\, \ell\left(d_{r,\Delta_i}^{(6)}\right), \tag{11.7}$$

where P_M denotes the transmit power, G_i is the fading and $\ell(d_{r,\Delta_i}^{(6)})$ refers to the path loss at distance $d_{r,\Delta_i}^{(6)}$, as specified in Eqs. (11.5) and (11.6), respectively. Each sum term can be regarded as a RV G_i, which is weighted by the factor $P_M \ell(d_{r,\Delta_i}^{(6)})$. Hence, the statistics of $I_6(r, \phi)$ outside the cell-center, i.e., $r > 0$, are accessible via a sum of differently weighted RVs. Since, in general, this does not lead to closed-form results, as detailed in Chap. 12, in this chapter a circular interference model is proposed in order to facilitate the statistical analysis.

11.3.1 Proposed Model

In the proposed circular interference model, the power of the six reference BSs is spread uniformly along a circle of radius R. This is achieved by evenly distributing the total transmit power $6 P_M$ among M equally spaced BSs and considering the limiting case $M \to \infty$. By generalizing Eq. (11.7), this is expressed as

$$I_C(r) = \lim_{M \to \infty} \frac{6 P_M}{M} \sum_{i=1}^{M} G_i \, \ell\left(d_{r,\Delta_i}^{(M)}\right) = \frac{6 P_M}{2\pi} \mathbb{E}\left[G_i\right] \int_{-\pi}^{\pi} \ell\left(d_{r,\Delta}\right) d\Delta, \quad (11.8)$$

with $\ell(\cdot)$ from Eq. (11.5) and $d_{r,\Delta_i}^{(M)}$ from Eq. (11.6). The terms $d_{r,\Delta}$ and Δ denote distance and angle-difference between the user and an infinitesimal interfering circular segment, as illustrated in Fig. 11.1.

Assuming a path loss exponent $\alpha = 2$, i.e., free space propagation, Eq. (11.8) can explicitly be evaluated as

$$I_C(r) = 6 P_M \mathbb{E}\left[G_i\right] \frac{1}{c_P} \frac{1}{R^2 - r^2}. \quad (11.9)$$

An intuitive interpretation of this result is provided in the next section by the model's pendant.

In the remainder of this chapter, $\alpha = 2$ is employed. It represents the worst case of low interference attenuation. However, previously- as well as all subsequently presented analysis can be carried out in closed-form for $\alpha = 2n$ with $n \in \mathbb{N}$. Values α other than these require the evaluation of elliptic integrals (see, e.g., [24]). Thus, a practical first order estimate for arbitrary values of α is achieved by evaluating the performance with $2n$ and $2(n + 1)$, where $2n < \alpha < 2(n + 1)$.

11.3.2 The Dual Model

Consider a user in a hexagonal scenario, which is moved along a circle of radius r from $-\pi$ to π, as indicated in Fig. 11.1. The *average expected* interference along the circle can be calulated as

$$I'_C(r) = \frac{1}{2\pi} \int\limits_{-\pi}^{\pi} \mathbb{E}\left[I_6(r, \phi')\right] d\phi' \tag{11.10}$$

$$= \sum_{i=1}^{6} P_\mathrm{M}\, \mathbb{E}\left[G_i\right] \frac{1}{2\pi} \int\limits_{-\pi}^{\pi} \ell(d_{r,\Delta}) d\phi'. \tag{11.11}$$

The result is obtained by plugging Eq. (11.7) into Eq. (11.10), exchanging sum and integral, and exploiting the linearity of the expectation. It is equivalent to $I_C(r)$ in Eq. (11.8) and, consequently, also yields Eq. (11.9). Thus, the result is *independent of the user's angle-position*. It can be interpreted as the *average expected* interference, i.e., the interference experienced by a *typical* user in a hexagonal scenario at distance r.

From Eq. (11.9) it is observed that the average expected interference increases by either increasing the transmit power P_M, decreasing the distance of the interferers R, or moving the user further away from the origin, which is reflected by the parameter r. The fading enters the equation only via the expectation, i.e., Eqs. (11.8) and (11.11) hold for arbitrary fading distributions with finite mean. Finally, note that the circular interference model is not restricted to hexagons. By replacing '6' by 'N' in Eqs. (11.7)–(11.11), it can generally be applied for substituting any convex regular N-polygonal model, as validated in Sect. 11.5.1.

11.4 Statistics of Aggregate Interference

In this section, aggregate interference in a hexagonal scenario with I.I.D. Gamma fading is investigated. Motivated by the findings in Sect. 11.1, it is proposed to approximate its statistics by a *single Gamma RV*. The corresponding shape- and scale parameters are dependent on the distance and can be determined by applying the previously presented circular model.

11.4.1 Interference Statistics at the Center

Assume I.I.D. Gamma fading with $G_i \sim \Gamma\left[k_0, \theta_0\right]$. Then, according to Sect. 11.3, interference can be considered as a sum of Gamma RVs, which are weighted by the factors $P_\mathrm{M}\, \ell(d_{r,\Delta_i}^{(6)})$, i.e., the received power without fading.

At the center of a hexagonal scenario (i.e., at $r = 0$), all weighting factors are equal, i.e., $P_\mathrm{M}\, \ell(d_{r,\Delta_i}^{(6)}) = P_\mathrm{M}\, \ell(R)$. By virtue of the scaling- and summation property of a Gamma RV (cf. Sect. 11.1), the resulting interference is distributed as

$$I_6(0, \phi) \sim \Gamma\left[6\, k_0, \theta_0 P_\mathrm{M} \ell(R)\right]. \tag{11.12}$$

11.4.2 Interference Statistics Outside the Center

Outside the center (i.e., at $r > 0$), the distances $d_{r,\Delta_i}^{(6)}$ and, thus, also the weighting factors $P_M \ell(d_{r,\Delta_i}^{(6)})$ generally differ from each other. Hence, a non-uniform impact of the interferers is observed. Then, the interference statistics are only accessible via evaluating the distribution of a sum of Gamma RVs with varying scale parameter. This method is particularized in Chap. 12.

The current chapter resorts to the following first order estimate. It is proposed to approximate the typically experienced interference distribution at distance r, $0 < r \le R/2$, by

$$\hat{I}(r) \sim \Gamma[\hat{k}(r), \hat{\theta}(r)]. \tag{11.13}$$

The rationale for this model are findings in prior work, where out-of-cell interference in stochastic networks is appropriately assessed by a Gamma distribution [11]. If it can be proven as accurate, it considerably facilitates further performance analysis by applying the methods in Sect. 11.1.

The distribution in Eq. (11.13) is fully determined by the distance-dependent shape- and scale parameters $\hat{k}(r)$ and $\hat{\theta}(r)$, respectively. In order to evaluate the two parameters, firstly the proposed circular interference model is employed to determine expectation and variance of $\hat{I}(r)$. Then, it is exploited that $\mathbb{E}[\hat{I}(r)] = \hat{k}(r)\,\hat{\theta}(r)$ and $\mathrm{Var}[\hat{I}(r)] = \hat{k}(r)\,\hat{\theta}^2(r)$.

As discussed in Sect. 11.3.1, the distinct received powers from the interfering BSs can be *averaged* along a circle of radius r. Thus, the typical impact of one interferer is calculated as

$$P_M \frac{1}{2\pi} \int_{-\pi}^{\pi} \ell(d_{r,\Delta})\, d\Delta = \frac{P_M}{c_P} \frac{1}{R^2 - r^2}, \tag{11.14}$$

and yields the average expected interference at distance r as

$$\mathbb{E}\left[\hat{I}(r)\right] = 6\,k_0\theta_0 \frac{P_M}{c_P} \frac{1}{R^2 - r^2}. \tag{11.15}$$

The variance of the aggregate interference comprises two components:

1. The variance of the fading, which calculates as

$$\mathrm{Var}_f\left[\hat{I}(r)\right] = 6\,k_0\left(\theta_0 \frac{P_M}{c_P} \frac{1}{R^2 - r^2}\right)^2. \tag{11.16}$$

2. The variance of the received power without fading, which is caused by the unequal distances d_{r,Δ_i}. With

$$\frac{1}{2\pi} \int_{-\pi}^{\pi} \left(P_{\mathrm{M}} \ell \left(d_{r,\Delta} \right) - P_{\mathrm{M}} \ell(R) \right)^2 d\Delta = \left(\frac{P_{\mathrm{M}}}{c_{\mathrm{P}} R^2} \right)^2 \frac{2r^2 R^4 + r^4 R^2 - r^6}{\left(R^2 - r^2 \right)^3},$$

$$(11.17)$$

the second variance component is obtained as

$$\mathrm{Var}_d \left[\hat{I}(r) \right] = 6k_0 \left(\theta_0 \frac{P_{\mathrm{M}}}{c_{\mathrm{P}} R^2} \right)^2 \frac{2r^2 R^4 + r^4 R^2 - r^6}{\left(R^2 - r^2 \right)^3}. \qquad (11.18)$$

Since the two components are statistically independent, the overall variance is calculated as

$$\mathrm{Var} \left[\hat{I}(r) \right] = \mathrm{Var}_f \left[\hat{I}(r) \right] + \mathrm{Var}_d \left[\hat{I}(r) \right]$$

$$= 6k_0 \left(\theta_0 \frac{P_{\mathrm{M}}}{c_{\mathrm{P}}} \frac{1}{R^2 - r^2} \right)^2 \left(1 + \frac{2r^2 R^4 + r^4 R^2 - r^6}{R^6 - r^2 R^4} \right) \qquad (11.19)$$

where $\mathrm{Var}_f[\hat{I}(r)]$ and $\mathrm{Var}_d[\hat{I}(r)]$ refer to Eqs. (11.16) and (11.18), respectively.

Finally, the distance-dependent shape- and scale parameter are derived from Eqs. (11.15) and (11.19) as

$$\hat{k}(r) = 6k_0 \frac{R^4 (R^2 - r^2)}{R^6 + r^2 R^4 + r^4 R^2 - r^6}, \qquad (11.20)$$

$$\hat{\theta}(r) = \theta_0 \frac{P_{\mathrm{M}}}{c_{\mathrm{P}}} \frac{1}{R^2 - r^2} \left(1 + \frac{2r^2 R^4 + r^4 R^2 - r^6}{R^6 - r^2 R^4} \right). \qquad (11.21)$$

11.5   Numerical Results and Discussion

In this section, the accuracy of the circular model and the proposed Gamma approximation are verified by numerical evaluation.

11.5.1   Validation of Expected Aggregate Interference

First, the expected interference powers in the hexagonal reference scenario and the proposed circular interference setup are compared to each other. The transmit power and inter-site distance are specified as $P_{\mathrm{M}} = 40$ W and $R = 500$ m, based on the standard 3rd Generation Partnership Project (3GPP) macro cell scenario from [23]. Intercept and constant of the path loss $\ell(\cdot)$ are set $b_{\mathrm{P}} = 1$ and $c_{\mathrm{P}} = 1$ for simplicity.

Table 11.1 System
parameters for validation.
Transmit power and circle
radius are referred from [23]

Parameter	Value
Transmit power	$P_M = 40\,W$
Circle radius	$R = 500\,m$
Path loss intercept	$b_P = 1$
Path loss constant	$c_P = 1$
Path loss exponent	$\alpha = 2$
Fading distribution	$G_i \sim \Gamma[1, 1]$

Fading is assumed to be distributed as $G_i \sim \Gamma[1, 1]$. The parameters are summarized
in Table 11.1.

Consider a user which is moved along a semi circle $\{(r, \phi)\,|\,\phi \in [0, \pi]\}$, as indicated in Fig. 11.1. The expected interference in the hexagonal scenario is calculated
as

$$\mathbb{E}\,[I_6(r, \phi)] = \sum_{i=1}^{6} P_M\,\mathbb{E}[G_i]\,\ell\left(d_{r,\Delta_i}^{(6)}\right), \qquad (11.22)$$

with $I_6(r, \phi)$ from Eq. (11.7) and $\mathbb{E}[G_i] = 1$. For the circular model, $\mathbb{E}\,[I_C(r)] = I_C(r)$, with $I_C(r)$ from Eq. (11.9).

Figure 11.2 depicts the evaluated results of Eqs. (11.9) and (11.22) for various
distances r. It is observed that

- At cell-center, i.e., at $r = 0$ m, the expected interference powers in the hexagonal-
and circular scenario ($\mathbb{E}[I_6(0, \phi)]$ and $I_C(0)$) are equal.
- Outside the center, i.e., at $r > 0$ m, $\mathbb{E}[I_6(r, \phi)]$ fluctuates around $I_C(r)$. The deviation is weak in the middle of the cell ($r = 125$ m), and strong at cell-edge

Fig. 11.2 Expected
aggregate interference
experienced at position (r, ϕ)
in circular- ($I_C(r)$) and
hexagonal model
($\mathbb{E}[I_6(r, \phi)]$), respectively.
Receiver distances
$r = \{0, 125, 250\}$ m refer to
cell-center, middle of cell
and cell-edge, respectively
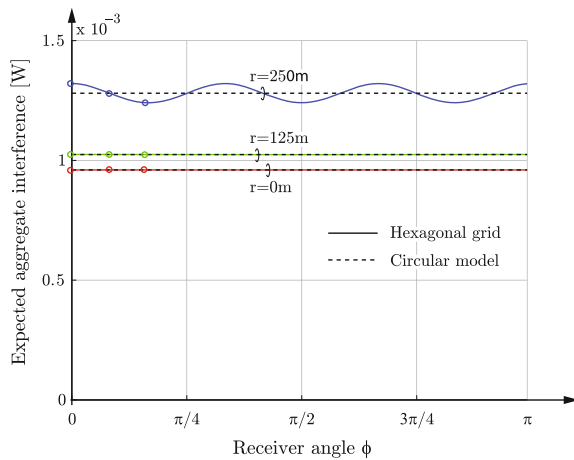
$(r = 250 \text{ m})$. Note that $\mathbb{E}[I_6(r, \phi)]$ is not symmetric about $I_C(r)$ due to the concavity of the path loss model.

The relative error of the circular interference model is calculated as

$$\varepsilon\,(r, \phi) = \left| \frac{\mathbb{E}\,[I_6(r, \phi)] - I_C(r)}{\mathbb{E}\,[I_6(r, \phi)]} \right|, \tag{11.23}$$

with $I_C(0)$ and $\mathbb{E}[I_6(0, \phi)]$ from Eqs. (11.9) to (11.22), respectively. The largest error occurs at cell-edge, i.e.,

$$\max_{r, \phi} \epsilon\,(r, \phi) = \max_{\phi} \epsilon\,(250, \phi). \tag{11.24}$$

In the specified scenario, $\max_{\phi} \epsilon\,(250, \phi) = 3.2\,\%$, as shown in Fig. 11.3.

11.5.2   Validation of Gamma Approximation

In this section, the accuracy of the Gamma approximation in Eq. (11.13) and its parameterization by Eqs. (11.20) and (11.21) are verified. The exact position-dependent distributions of $I_6(r, \phi)$ are obtained by evaluating Theorem 12.1.

In order to capture a *representative* profile of distributions, three user distances $r = \{0, 125, 250\}$ m and three angle-positions $\phi = \{0, \frac{\pi}{12}, \frac{\pi}{6}\}$ are considered, as illustrated by bold dots in Fig. 11.4. The distances correspond to cell-center, middle of cell and cell-edge, respectively. The angle $\phi = 0$ represents a user, which is moved

Fig. 11.3 Maximum deviation of circular interference model from expected interference in *convex regular N-polygonal* models. The labeled cell-shapes can be arranged in a grid without overlapping areas
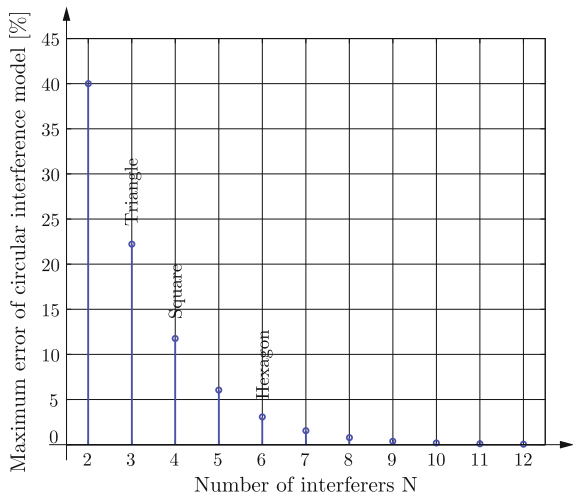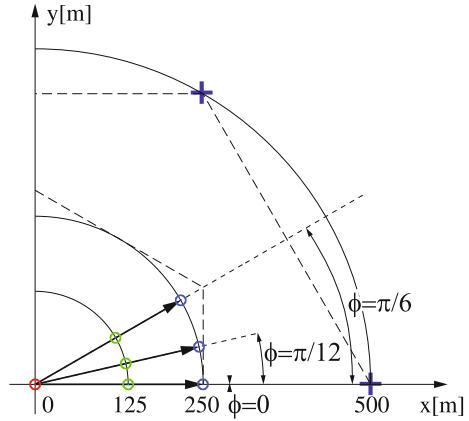
Fig. 11.4 Setup for
evaluation. Cutout of
Fig. 11.1 (*upper right*
quadrant)

directly towards its strongest interferer, $\phi = \frac{\pi}{6}$ refers to the path with two equidistant
dominant interferers, and $\phi = \frac{\pi}{12}$ is a variation thereof.

Fading is specified as $G_i \sim \Gamma[2, 1]$. This corresponds to a 1×2 Single-Input
Multiple-Output SIMO system with Rayleigh-fading and Multiple-Input Single-
Output (MISO) at the user, or, equivalently, a 2×1 MISO system with MRT at
the BS.

The Cumulative Distribution Function (CDF) of the Gamma approximation,
$F_{\hat{I}}(x; \hat{k}(r), \hat{\theta}(r))$ and the CDF $F_6(x; r, \phi)$ of $I_6(r, \theta)$ are evaluated at each distance
r and angle ϕ, respectively. The accuracy of the Gamma approximation is *quantified*
by Kolmogorov–Smirnov KS statistics, which formulate as

$$D_{\text{KS}}(r, \phi_m) = \sup_{x} \left| F_{\hat{I}}\left(x; \hat{k}(r), \hat{\theta}(r)\right) - F_6\left(x; r, \phi\right) \right|. \qquad (11.25)$$

Results are depicted in Fig. 11.5. The Gamma approximation most closely resem-
bles the experienced interference distributions at $\phi = \frac{\pi}{12}$. In this case, the difference
between exact- and approximated CDFs is less than 1 % for $r < 159$ m and 2.75 %
at cell-edge ($r = 250$ m). The largest deviation occurs at $\phi = \frac{\pi}{6}$, where the user is
moved centrally in between its two dominant interferers (upper curve). Then, the
distributions differ by less than 1 % for $r < 155$ m and by 3.7 % at cell-edge.

For *qualitative* evaluation, Fig. 11.6 depicts the exact CDFs and the corresponding
Gamma approximations at the specified representative user positions, which are
denoted by bold dots in Figs. 11.4 and 11.5, respectively.

The Gamma CDFs perfectly fit at cell center ($r = 0$ m) and in the middle of the cell
($r = 125$ m). At cell-edge ($r = 250$ m), the Gamma approximation closely resem-
bles the experienced interference of a user at $\phi = \frac{\pi}{12}$. The probability of high inter-
ference values at $\phi = \frac{\pi}{6}$ is slightly underestimated by at most 3.7 % (cf. Fig. 11.5).

Fig. 11.5 KS statistics at position (r, ϕ_m), comparing Gamma approximation and exact distribution. Receiver distances $r = \{0, 125, 250\}$ m refer to cell-center, middle of cell and cell-edge, respectively
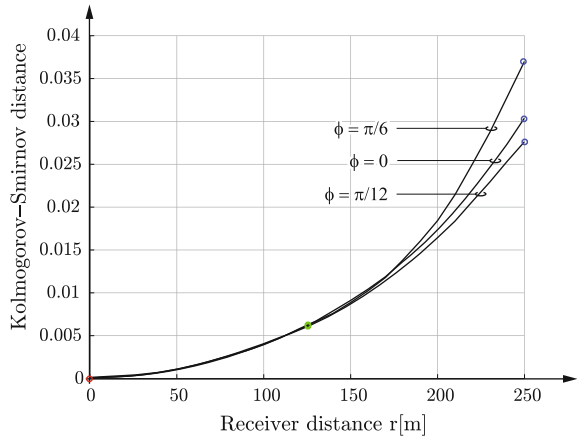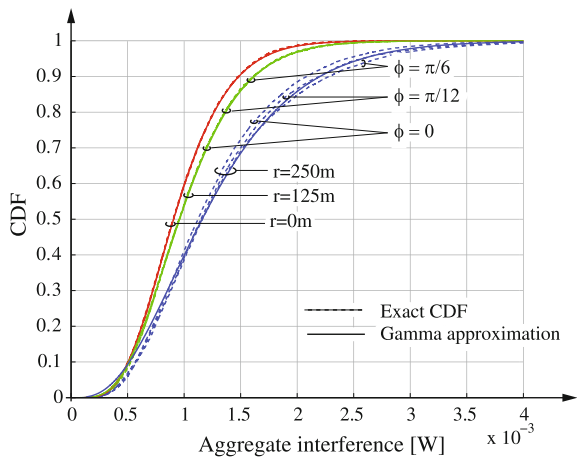

Fig. 11.6 Aggregate interference at particular user positions (see *bold dots* in Fig. 11.4): Exact CDFs, as obtained by numerically evaluating [25] for a hexagon scenario *dashed lines* and corresponding Gamma approximations *solid lines*

11.6   Application in Heterogeneous Networks

In this section, aggregate interference statistics in a two-tier heterogeneous cellular network with regularly placed macro-BSs and randomly distributed small cell BSs are investigated. The interference contribution from each tier is approximated by a single Gamma RV and the total interference is calculated as the sum of the two. The accuracy of the approximations is verified by extensive Monte Carlo simulations.

The macro-tier comprises six hexagonally arranged BSs at distance $R = 500$ m, each transmitting with $P_M = 40$ W. Small cell BSs are distributed according to a Poisson Point Process PPP of density $\mu_S = 10^{-4}$ m^{-2} and transmit with a power of $P_S = 0.4$ W. As indicated in Fig. 11.7, they are excluded from a ball (in fact, it is a disc, but *ball* is the more common term in literature, e.g., in [11]) of radius $R_{Ex} = (P_M/P_S)^{-1/\alpha} R/2$ around the user so as to ensure user association to the central

Fig. 11.7 Snapshot of a
heterogeneous network
deployment. Macro-BSs are
arranged on a hexagon.
Small cell BSs are randomly
distributed around a user at
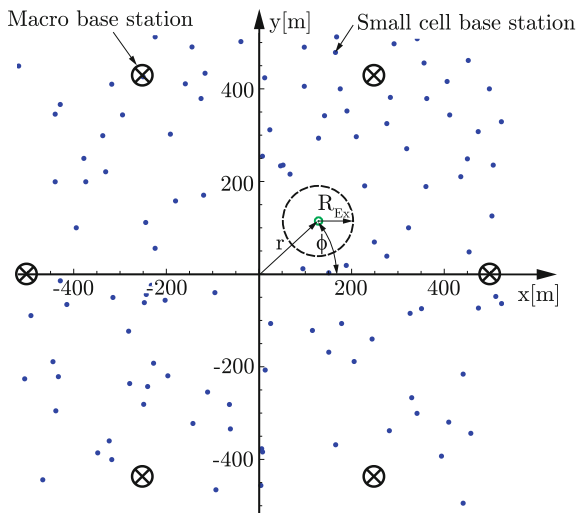(r, ϕ) and excluded from a
ball of radius R_{Ex}

Table 11.2 Parameters for
numerical evaluation of
heterogeneous scenario

Parameter	Value
Macro-BS transmit power	$P_M = 40\,\text{W}$
Inter macro-site distance	$R = 500\,\text{m}$
Small cell BS transmit power	$P_S = 0.4\,\text{W}$
Small cell density	$\mu_S = 10^{-4}\text{m}^{-2}$
Path loss intercept	$b_P = 1$
Path loss constant	$c_P = 1$
Path loss exponent	$\alpha = 4$
Fading distribution	$G_i \sim \Gamma[1, 1]$

macro-BS at cell-edge. In both tiers, the path loss $\ell(\cdot)$ is modeled according to
Eq. (11.5), with intercept $b_P = 1$, constant $c_P = 1$ and exponent $\alpha = 4$. Fading is
assumed to be distributed as $G_i \sim \Gamma[1, 1]$. The parameters are summarized in
Table 11.2.

In the first step, the interference contribution from the macro-tier is approximated
by a Gamma RV $\hat{I}_M(r) \sim \Gamma[\hat{k}_M(r), \hat{\theta}_M(r)]$. According to Sect. 11.4, it can be para-
meterized by the circular interference model. Recalculating Eqs. (11.15), (11.16),
(11.18) and (11.19) for $\alpha = 4$ yields

$$\hat{k}_M(r) = \frac{6\,k_0 R^8 \left(r^2 - R^2\right) \left(r^2 + R^2\right)^2}{r^{14} - 7r^{12}R^2 + 23r^{10}R^4 - 41r^8R^6 + 39r^6R^8 - 25r^4R^{10} - 9r^2R^{12} - R^{14}},$$
(11.26)

$$\hat{\theta}_M(r) = \frac{\theta_0 P_M \left(-r^{14} + 7r^{12}R^2 - 23r^{10}R^4 + 41r^8R^6 - 39r^6R^8 + 25r^4R^{10} + 9r^2R^{12} + R^{14}\right)}{c_P \left(r^2 - R^2\right)^4 \left(r^2 + R^2\right) R^8}.$$
(11.27)

Secondly, the contribution of the small cell tier is also approximated by a Gamma RV $\hat{I}_S \sim \Gamma[\hat{k}_S, \hat{\theta}_S]$. Along the lines of [26, Eqs. (2.19) and (2.21)], mean and variance of the actual interference $I_{A,S}$ from the PPP model are determined as

$$\mathbb{E}[I_{A,S}] = P_S \, \mathbb{E}[G_i] 2\pi \, \mu_S \int_{R_{Ex}}^{\infty} r \, \ell(r) dr$$

$$= P_S \, k_0 \, \theta_0 \frac{1}{c_P} \pi \, \mu_S \, R_{Ex}^{-2}, \qquad (11.28)$$

$$\text{Var}[I_{A,S}] = \mathbb{E}[G_i^2] 2\pi \, \mu_S \int_{R_{Ex}}^{\infty} r \, \ell(r)^2 dr$$

$$= (1 + k_0) k_0 \, \theta_0^2 \, P_S^2 \frac{1}{c_P^2} \frac{\mu_S \pi}{3} R_{Ex}^{-6}. \qquad (11.29)$$

Then, exploiting the identities $\mathbb{E}[\hat{I}_S] = \hat{k}_S \, \hat{\theta}_S$ and $\text{Var}[\hat{I}_S] = \hat{k}_S \, \hat{\theta}_S^2$ yields

$$\hat{k}_S = \frac{3 R_{Ex}^2 \, k_0 \, \theta_0 \, \mu_S}{(1 + k_0)}, \qquad (11.30)$$

$$\hat{\theta}_S = \frac{P_S (1 + k_0)}{3 \, c_P \, R_{Ex}^{\alpha}}. \qquad (11.31)$$

Finally, the PDF of the total aggregate interference, $\hat{I}_A(r) = \hat{I}_M(r) + \hat{I}_S$, at user distance r is calculated as

$$f_{\hat{I}_A}(x; r) = \hat{\theta}_M(r)^{-\hat{k}_M(r)} \hat{\theta}_S^{-\hat{k}_S} e^{-\frac{x}{\hat{\theta}_S}} x^{\hat{k}_M(r) + \hat{k}_S - 1}$$

$$\times \, {}_1\tilde{F}_1\left(\hat{k}_M(r); \hat{k}_M(r) + \hat{k}_S; \left(\frac{1}{\hat{\theta}_S} - \frac{1}{\hat{\theta}_M(r)}\right) x\right), \qquad (11.32)$$

where ${}_1\tilde{F}_1(\cdot; \cdot; \cdot)$ denotes the regularized confluent hypergeometric function.

In order to verify the accuracy of this approximation, Monte Carlo simulations are carried out. The results for a *typical* user at distance r are obtained by averaging over 10^6 uniformly distributed angle-positions on $[0, 2\pi]$. For each position, 10^5 fading- and 10^4 spatial realizations of the small cell deployment are generated. The small cell BSs are distributed over a circular area of radius $10R$.

Figure 11.8a depicts the individual interference contributions from the macro- and the small cell tier at various user distances r. It is observed that the CDFs for the macro tier, which correspond to the approximation in Eqs. (11.26), and (11.27), show an accurate fit with the Monte Carlo simulations. This corroborates the claim in Sect. 11.3.1 that the circular model is also applicable for path loss exponents other than $\alpha = 2$. The interference CDF of the small cell tier, which refers to the approximation in Eqs. (11.30) and (11.31), is independent of the user distance r due to the fixed exclusion radius R_{Ex}. It is also in close agreement with the simulations. Figure 11.8b shows the CDFs of the aggregate interference from both macro- and

Fig. 11.8 CDFs of interference from macro- and small cell tier **a** and aggregate interference from both tiers **b**. *Solid lines* indicate results as obtained by approximating the contribution of each tier by a Gamma RV. *Dashed lines* show results from Monte Carlo simulations. User distances $r = \{0, 125, 250\}$ m refer to cell-center, middle of cell and cell-edge, respectively
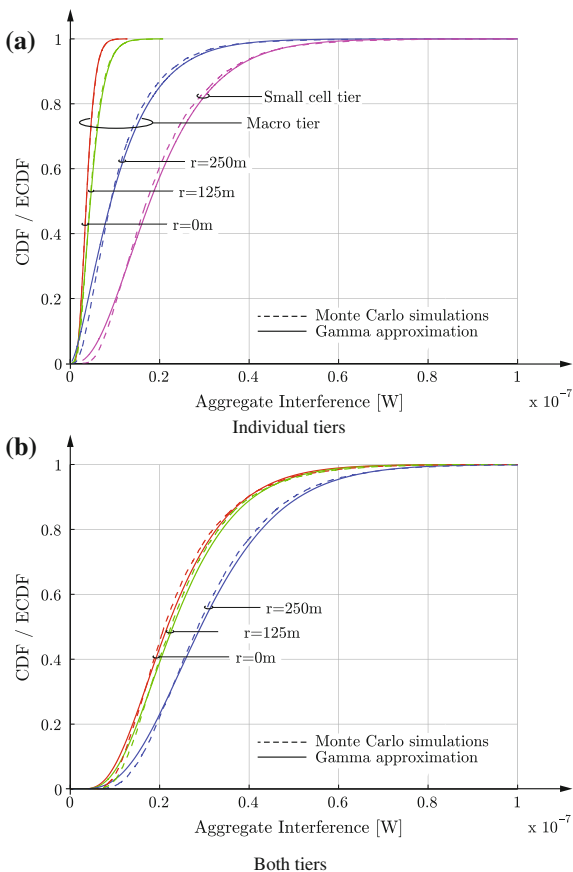
small cell tier. It is found that the approximation by a sum of two independently parameterized Gamma RVs almost perfectly captures the actual interference characteristics at the cell center ($r = 0$ m) and in the middle of the cell ($r = 125$ m). It even provides an accurate fit at cell-edge ($r = 250$ m).

11.7   LTE-Advanced System Level Simulations

In this section, the validity of the Gamma distribution for approximating aggregate interference in symmetric interference scenarios is evaluated. In the first part, the corresponding system model is introduced.

11.7.1 System Model

The system model is composed of a central macro site and six neighboring nodes, which are arranged according to a hexagonal grid, as illustrated in Fig. 11.9. Each site employs a single eNodeB, which is equipped with an omni-directional antenna. For systematic investigations, the UEs are equidistantly distributed along concentric circles of radius $r = \{50, 120, 210\}$ m, referring to cell-center, middle of cell and cell-edge, respectively. Each circle encompasses 24 UEs, which are uniquely identified by the tuple (r, ϕ), where ϕ denotes the angle position. The signal experiences free-space path loss, fast fading according to a time-correlated Rayleigh channel, and spatially-correlated log-normal shadowing with 8 dB standard deviation. Hereinafter, the combination of these three mechanisms is termed *composite fading*. The free-space path loss law is defined as $\min(b_P, 1/c_P d^{-2})$. In this section, $b_P = 10^{-7}$ and $f_c = 2.14$ GHz, yielding $c_P = (4\pi f_c/c_0)^2 = 8.0465 \times 10^3$, where c_0 is the speed of light. The shadow fading maps are computed by applying the method in [27]. The results in this section are obtained by averaging over 100 channel realizations and 100 TTIs. The simulation parameters are summarized in Tables 9.6 and 11.3, respectively.

Fig. 11.9 *Hexagonal grid* setup with central cell and six interfering eNodeBs. UEs are equidistantly distributed along circles of radius r = {50, 120, 210} m. *Bold dots* indicate representative UE positions. The corresponding angles are given by $\phi = \{0, \frac{\pi}{12}, \frac{\pi}{6}\}$, respectively. In the case of BS collaboration, eNodeB 7 does not contribute to the aggregate interference
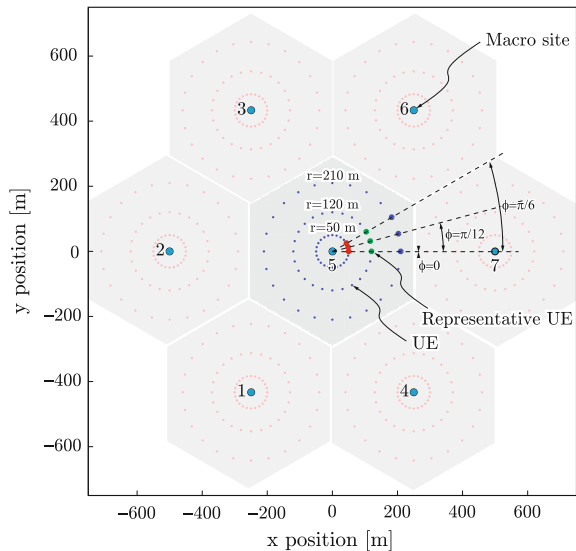
Table 11.3 Specific parameters for simulations of homogeneous macro cellular network

Parameter	Value
Antenna configuration	$N_{Tx} \times N_{Rx} = 1 \times 1$
eNodeB antenna gain in dB	$A(\theta) = 0$ dB
Path loss	$\ell(d) = \min(b_P, 1/c_P d^{-2})$
Scheduler type	Round robin

### 11.7.2 Validation of Gamma Approximation

In this section, the introduced circular interference model is validated. The particular focus lies on the accuracy of the Gamma distribution as an approximation for both composite fading and aggregate interference. The system model is referred from Sect. 11.7.1.

Firstly, the average aggregate interference is measured along each of the three UE circles. The results are depicted as solid lines in Fig. 11.10. In accordance with Sect. 11.5.1, it is observed that average aggregate interference is almost constant at the cell-center and in the middle of the cell. At cell-edge, the curves exhibit fluctuations due to the vicinity of the dominant interferers. Results from the circular interference model accurately assess the average behavior, as shown by the dashed lines.

In the next step, the Empirical Cumulative Distribution Function (ECDF) of the aggregate interference is computed at nine representative UE locations, which are marked by bold dots in Fig. 11.9. Similar to Sect. 11.5.2, the angle positions $\phi = \{0, \frac{\pi}{6}, \frac{\pi}{12}\}$ refer to UEs with one dominant interferer (eNodeB 7), two equidistant dominant interferers (eNodeBs 6 and 7) and a variation thereof. Solid lines in Fig. 11.11 depict the results. In accordance with Sect. 11.5.2, the interference distributions are dominated by the UEs' distances to the origin while their angle positions have only minor impact. The latter is illustrated by the enlarged section in Fig. 11.11.

Finally, the introduced circular model is applied to approximate the aggregate interference distribution at a certain distance r by a Gamma RV. The first step consists in determining the parameters k_0 and θ_0 of the Gamma distribution $\Gamma[k_0, \theta_0]$ that models the composite fading (cf. Sect. 11.4). This is achieved by applying Algorithm 2. The initial values k_0' and θ_0' are obtained from Maximum Likelihood Estimation (MLE). MLE maximizes the *likelihood* $\mathcal{L}(k_0', \theta_0'|x) = f(x|k_0', \theta_0')$, where $f(\cdot)$ denotes a Gamma PDF with shape k_0' and scale θ_0', and x are the given outcomes.

Fig. 11.10 Average aggregate interference power along the three UE circles in Fig. 11.9. *Solid curves* refer to simulation results, *dashed curves* denote results from circular interference model
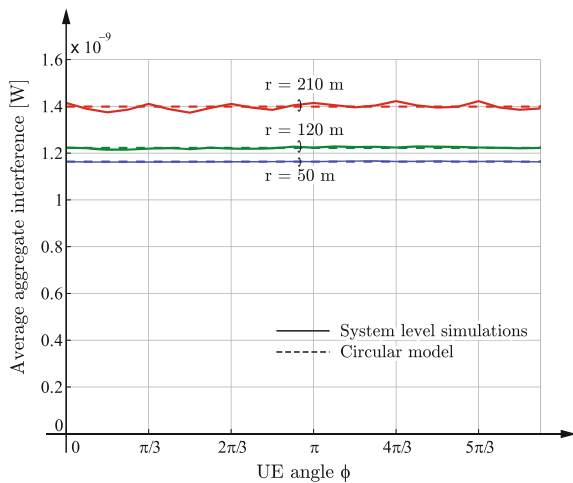
Using a step size of $\Delta = 0.001$ and $N_{\text{iterations}} = 100$ yields a KS distance of 0.0512 between simulated- and approximated composite fading distribution. For comparison, employing only MLE achieves a KS distance of 0.0917.

Algorithm 2: Iterative algorithm for improving KS distance between empirical composite fading distribution and Gamma approximation. The term $F(x; k, \theta)$ denotes the CDF of a Gamma distribution with shape k and scale θ, respectively.

Data: empirical CDF of composite fading from simulations: $F_{\text{fading}}(x)$;
   initial shape- and scale parameter: k_0', θ_0';
   stepsize: Δ;
   number of iterations: $N_{\text{iterations}}$;
Result: shape- and scale parameter: k_0, θ_0;
set $k_0 = k_0'$ and $\theta_0 = \theta_0'$;
for $i = 1$ **to** $N_{\text{iterations}}$ **do**
 compute $\{k^*, t^*\} = \arg\min_{\{k,t\}} \sup_x |F_{\text{fading}}(x) - F(x; k, \theta)|$, with
 $k \in [k_0 - \Delta, k_0, k_0 + \Delta]$ and $\theta \in [\theta_0 - \Delta, \theta_0, \theta_0 + \Delta]$;
 if k^* *equals* k_0 **and** θ^* *equals* θ_0 **then**
  | break;
 else
  | set $k_0 = k^*$ and $\theta_0 = \theta^*$;
 end
end

Then, for each UE distance, the parameters of the aggregate interference distribution, $\hat{k}(r)$ and $\hat{\theta}(r)$, are calculated with Eqs. (11.20) and (11.21), respectively. The corresponding CDF curves are depicted as dashed lines in Fig. 11.11. It is observed that the approximated distributions slightly underestimate the occurrence of high interference values. In order to quantify the deviation from the simulated curves,

Fig. 11.11 Aggregate interference distributions at representative UE locations $r = \{50, 120, 210\}$ m and $\phi = \{0, \frac{\pi}{12}, \frac{\pi}{6}\}$, as marked by bold dots in Fig. 11.9. *Solid lines* refer to ECDF curves from simulations, *dashed lines* denote Gamma approximations as obtained with circular model
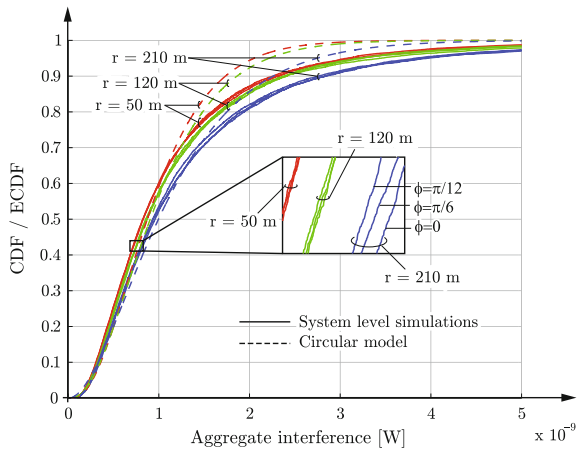
Table 11.4 KS distances between Gamma approximations and simulated ECDF curves at representative UE locations

	$\phi = 0$	$\phi = \frac{\pi}{12}$	$\phi = \frac{\pi}{6}$
r = 50 m	0.0713	0.0768	0.0762
	0.1391	0.1491	0.1454
	0.0720	0.0797	0.0773
r = 120 m	0.0697	0.0659	0.0698
	0.1347	0.1393	0.1300
	0.0815	0.0708	0.0701
r = 210 m	0.0565	0.0496	0.0466
	0.1183	0.1289	0.1274
	0.0823	0.0828	0.0840

For each r, the first two rows correspond to the Gamma approximation as obtained with the circular model. In the first row, composite fading is estimated with Algorithm 2, while in the second row it is assessed with MLE, respectively. The third row refers to the direct application of MLE on the distribution of the aggregate interference

the first row in Table 11.4 provides the KS distance for each UE location (r, ϕ). The values range from 0.05 at $r = 210$ m to 0.08 at $r = 50$ m.

For comparison, each simulated curve is also approximated by two further Gamma distributions. The first distribution adapts the circular model and estimates the composite fading by MLE, i.e., it employs the parameters k_0 and θ_0 that were used above to initialize Algorithm 2. The second distribution is computed by applying MLE directly to the simulated aggregate interference. The corresponding KS distances are likewise listed in the second- and third row of Table 11.4 for each UE location (r, ϕ). The first observation is that Algorithm 2 considerably improves the performance of the circular model, such that it even exceeds pure MLE of the aggregate interference. Hence, the accuracy of the circular model crucially depends on the precision of the composite fading approximation. Secondly, the results of the MLE range from 0.07 to 0.08, indicating that the assumption of Gamma-distributed interference itself induces a systematic error.

In summary, the circular model achieves a remarkable accuracy of fit despite its simplicity, thus corroborating its applicability.

11.8 Conclusion

In this chapter, a circular interference model for aggregate interference analysis in regular grid deployments is introduced. Particular focus is placed on characterizing a user at an eccentric location. The expected interference from the circular model is identified as the interference that is experienced by a typical user in a hexagonal grid at a certain distance from the origin. At cell-edge, it deviates by at most 3.2 % from the actual values.

In a second step, the corresponding interference statistics are approximated by a single Gamma RV. By means of the circular model, the distance-dependent shape- and scale parameters are determined in closed form and unveil the two key formative components of the distribution as the variance of the fading and the variance of the path loss due to the eccentric user location, respectively. Qualitative- and quantitative comparisons with the exact distributions confirm the accuracy of the Gamma approximation, yielding KS statistics no higher than 3.7 %.

The circular model's expedient adaption for representing the *well-planned part* of a two-tier heterogeneous cellular network is demonstrated. The example merges a fully regular macro-deployment with completely randomly distributed small cells and models the interference contribution from each tier by a single Gamma RV. The resulting aggregate interference distribution shows a remarkably good fit with Monte Carlo simulations. Hence, the model enables to accurately capture the impact of *both* user eccentricity *and* heterogeneity of the network with only few key parameters.

In the last part of the chapter, it is shown that the circular model enables an accurate prediction of the interference statistics in an LTE-A hexagonal grid scenario. Deviations from the simulation results mainly stem from the inaccurate approximation of the composite fading. The remainder of the approximation error is caused by the assumption of Gamma distributed aggregate interference itself.

The presented circular model does not allow to account for power control and coordination among BSs. This is a major motivation for the next chapter, which extends the model by non-uniform power profiles.

References

1. J. Gertner, *The Idea Factory: Bell Labs and the Great Age of American Innovation* (Penguin Group, New York, 2012)
2. P. Marsch, G. Fettweis, Static clustering for cooperative multi-point (CoMP) in mobile communications, in *IEEE International Conference on Communications* (*ICC*) Kyoto, June (2011). doi:10.1109/icc.2011.5963458
3. C. Ball, R. Mullner, J. Lienhart, H. Winkler, Performance analysis of closed and open loop MIMO in LTE, in *European Wireless Conference* (*EW*), pp. 260–265, Aalborg, May (2009). doi:10.1109/EW.2009.5358012
4. A. Farajidana, W. Chen, A. Damnjanovic, T. Yoo, D. Malladi, C. Lott, 3GPP LTE downlink system performance, in *IEEE Global Telecommunication Conference* (*GLOBECOM*) Honolulu, December (2009). doi:10.1109/GLOCOM.2009.5425327
5. J. Giese, M. Amin, S. Brueck, Application of coordinated beam selection in heterogeneous LTE-advanced networks, in *International Symposium on Wireless Communications Systems* (*ISWCS*), pp. 730–734, Aachen, November (2011)
6. Y. Liang, A. Goldsmith, G. Foschini, R. Valenzuela, D. Chizhik, Evolution of base stations in cellular networks: denser deployment versus coordination, in *IEEE International Conference on Communications* (*ICC*), pp. 4128–4132, Beijing, May (2008). doi:10.1109/ICC.2008.775
7. T. Novlan, R. Ganti, J. Andrews, Coverage in two-tier cellular networks with fractional frequency reuse, in *IEEE Global Telecommunications Conference* (*GLOBECOM*), Houston, December (2011). doi:10.1109/GLOCOM.2011.6133767

8. F. Di Salvo, A characterization of the distribution of a weighted sum of Gamma variables through multiple hypergeometric functions. Integral Transforms Special Funct. **19**(8), 563–575 (2008). doi:10.1080/10652460802045258

9. M. Haenggi, J. Andrews, F. Baccelli, O. Dousse, M. Franceschetti, Stochastic geometry and random graphs for the analysis and design of wireless networks. IEEE J. Sel. Areas Commun. **27**(7), 1029–1046 (2009). doi:10.1109/JSAC.2009.090902

10. M. Haenggi, *Stochastic Geometry for Wireless Networks* (Cambridge University Press, Cambridge, 2012)

11. R.W. Heath Jr., M. Kountouris, T. Bai, Modeling heterogeneous network interference using Poisson point processes. IEEE Trans. Signal Process. **61**(16), 4114–4126 (2013). doi:10.1109/TSP.2013.2262679

12. Y. Zhuang, Y. Luo, L. Cai, J. Pan, A geometric probability model for capacity analysis and interference estimation in wireless mobile cellular systems, in *IEEE Global Telecommunications Conference* (*GLOBECOM*) Houston, December (2011). doi:10.1109/GLOCOM.2011.6134503

13. K.B. Baltzis, Hexagonal vs Circular Cell Shape: A Comparative Analysis and Evaluation of the Two Popular Modeling Approximations, *Cellular Networks-Positioning, Performance Analysis, Reliability* (InTech, Rijeka, 2011). doi:10.5772/626

14. M. Taranetz, M. Rupp, A circular interference model for wireless cellular networks, in *Proceedings of the International Wireless Communications & Mobile Computing Conference*, Nicosia (2014)

15. M. Taranetz, System level modeling and evaluation of heterogeneous cellular networks, Ph.D. dissertation, Institute of Telecommunications, TU Wien (2015). http://theses.eurasip.org/theses/611/system-level-modeling-and-evaluation-of/

16. I. Kostic, Analytical approach to performance analysis for channel subject to shadowing and fading. IEEE Proc. Commun. **152**(6), 821–827 (2005)

17. S. Al-Ahmadi, H. Yanikomeroglu, On the approximation of the generalized-K PDF by a gamma PDF using the moment matching method, in *IEEE Wireless Communications and Networking Conference* (*WCNC*) Budapest, April (2009). doi:10.1109/WCNC.2009.4917849

18. S. Al-Ahmadi, H. Yanikomeroglu, On the use of high-order moment matching to approximate the generalized-K distribution by a gamma distribution, in *IEEE Global Telecommunication Conference* (*GLOBECOM*) Honolulu, November (2009). doi:10.1109/GLOCOM.2009.5425259

19. J. Zhang, M. Matthaiou, Z. Tan, H. Wang, Performance analysis of digital communication systems over composite $\eta - \mu$ gamma fading channels. IEEE Trans. Veh. Technol. **61**(7), 3114–3124 (2012). doi:10.1109/TVT.2012.2199344

20. R.W. Heath Jr., T. Wu, Y.H. Kwon, A. Soong, Multiuser MIMO in distributed antenna systems with out-of-cell interference. IEEE Trans. Signal Process. **59**(10), 4885–4899 (2011). doi:10.1109/TSP.2011.2161985

21. S. Kusaladharma, C. Tellambura, Aggregate interference analysis for underlay cognitive radio networks. IEEE Wireless Commun. Lett. **1**(6), 641–644 (2012). doi:10.1109/WCL.2012.091312.120600

22. C.A. Coelho, J.T. Mexia, On the distribution of the product and ratio of independent generalized gamma-ratio random variables. Sankhyā: Indian J. Statist. **69**(12), 221–255 (2007)

23. 3rd Generation Partnership Project (3GPP), Evolved universal terrestrial radio access (E-UTRA); radio frequency (RF) system scenarios, in *3rd Generation Partnership Project* (*3GPP*), TR 36.942, October (2014)

24. I.S. Gradshteyn, I.M. Ryzhik, *Table of Integrals, Series, and Products*, 7th edn. (Elsevier/Academic Press, Amsterdam, 2007)

25. P. Moschopoulos, The distribution of the sum of independent gamma random variables. Ann. Inst. Statist. Math. **37**(1), 541–544 (1985)
26. F. Baccelli, B. Blaszczyszyn, *Stochastic Geometry and Wireless Networks: Volume I Theory*, Foundation and Trends in Networking (Now Publishers, Hanover, 2009). doi:10.1561/1300000006
27. H. Claussen, Efficient modelling of channel maps with correlated shadow fading in mobile radio systems, in *IEEE International Symposium on Personal, Indoor and Mobile Radio Communications* (*PIMRC*), vol. 1, pp. 512–516, Berlin, September (2005)